Ocean Engineering 350 (2026) 124030

Contents lists available at ScienceDirect

Ocean Engineering

journal homepage: www.elsevier.com/locate/oceaneng

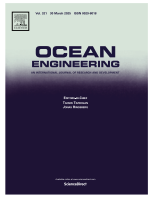

Research Paper

Estimating semi-stationary sea states through wavelet-based adaptive segmentation of ship motions

Taiyu Zhang [a], Can Ma [a], Yang An [a], Zhengru Ren [b,c,*]

[a] Institute for Ocean Engineering, Shenzhen International Graduate School, Tsinghua University, Tsinghua Campus, University Town, Shenzhen, 518055, China
[b] State Key Laboratory of Ocean Engineering, Shanghai Jiao Tong University, Shanghai, 200240, China
[c] School of Ocean and Civil Engineering, Shanghai Jiao Tong University, Shanghai, 200240, China

ARTICLE INFO

Keywords:
Sea state estimation
Wave buoy analogy
Semi-stationary waves
Adaptive segmentation

ABSTRACT

Environmental information is vital for the safety of marine operations, with waves being the primary external force affecting floating structures. Accurate sea state estimation enhances safety and efficiency in offshore activities, particularly as ocean engineering becomes increasingly complex. The wave buoy analogy (WBA) utilizes ship motion data to estimate wave energy distribution, offering a cost-effective and flexible solution for real-time monitoring. Although non-stationary ocean waves are often approximated as stationary for large-scale observations, the simplification can introduce potential inaccuracies and uncertainties in WBA technologies. It overlooks the inherent time-involved nature of waves, leading to errors in real-time applications of the WBA. To address these challenges, semi-stationary sea states are defined, and a wavelet-based adaptive segmentation algorithm is proposed for time-dependent sea state estimation, mitigating the inaccuracies inherent in traditional stationary assumptions. Simulations demonstrate the effectiveness of the proposed approach.

1. Introduction

Environmental information is critical for ensuring the safety of various marine operations (Fossen, 2011; Ren et al., 2021b; Wang et al., 2025). Among external forces, waves are the most dominant factor affecting floating structures. As a result, sea state estimation is essential for maintaining safety, improving efficiency, and supporting decision-making in offshore crane operations, pile driving, and other marine activities. It becomes especially important given the increasing scale and complexity of modern marine operations (Ren et al., 2021c; Ma et al., 2024; Yan et al., 2025).

Conventional observation methods such as satellite, wave rider buoys, and ship-borne wave radar are commonly used for monitoring wave conditions. However, airborne observations often introduce significant time delays and provide lower resolution (Martin, 2014), which may not be adequate for marine activities that require real-time support and low-risk tolerance. Wave rider buoys are one of the most commonly used solutions for wave monitoring, offering accurate wave parameters by processing data from accelerometers. However, their complex deployment and retrieval make them better suited for long-term service than for marine operations that require frequent relocation. Ship-borne wave radar, typically X-band radar, is a powerful tool that offers real-time updates while being able to move with the ship (Huang et al., 2017). However, its high cost and frequent calibration requirements result in a relatively low deployment rate. The wave buoy analogy (WBA) aims to extract valuable sea state information by using ship motions as input. It estimates the on-site distribution of wave energy by analyzing readily accessible ship responses (Iseki and Ohtsu, 2000; Tannuri et al., 2003). This approach balances real-time capabilities with flexibility, and due to the widespread installation of motion sensors, it can achieve near-zero-cost observations. As a result, the WBA serves as a valuable supplement to traditional sea state observation methods, offering a more flexible and responsive solution for real-time monitoring during marine operations.

The concept and mathematical formulation of wave estimation from ship motions are initially proposed by Iseki and Ohtsu (2000), Tannuri et al. (2003). Through years of development, it has become widely adopted within the community and continues to evolve with advancements in technology and methodology (Nielsen et al., 2023a). Parametric and non-parametric approaches are two options for solving the ill-posed sea state estimation problem. Parametric approaches rely on predefined wave spectrum shape, such as JONSWAP and Bretschneider, which limit adaptability and flexibility. Nonparametric approaches, on the other hand, are free from the limitations of predefined spectrum

* Corresponding author.
E-mail addresses: taiyu.zhang@outlook.com (T. Zhang), ma-c24@mails.tsinghua.edu.cn (C. Ma), anyang@sz.tsinghua.edu.cn (Y. An), ren.zhengru@sjtu.edu.cn (Z. Ren).

https://doi.org/10.1016/j.oceaneng.2025.124030
Received 24 June 2025; Received in revised form 15 December 2025; Accepted 16 December 2025
Available online 11 January 2026

shapes and can directly provide the distribution of wave power, offering a more accurate and flexible solution. Additionally, WBA techniques can be categorized into model-based and data-driven approaches, based on the requirement for wave-response transfer functions, i.e., the response amplitude operators (RAOs) (Majidian et al., 2022).

In model-based approaches, the linear assumption is applied to simplify the ship's response to waves as a linear superposition of individual wave components. RAO serves as the transfer function, with the sea state estimation framed as an inverse problem to be solved. The Bayesian framework provides a powerful method for integrating prior information with observational data, offering a robust and transparent way to estimate sea conditions while explicitly accounting for uncertainties (Nielsen, 2008; Mas-Soler and Simos, 2020). Different variants of Kalman filters are employed to solve the inverse problem of sea state estimation in real time. The Kalman filter efficiently integrates new data into the existing estimate while accounting for uncertainties in both the model and the measurements, offering a robust solution (Pascoal and Guedes Soares, 2009; Kim et al., 2019; Peng et al., 2019). Optimization methods provide another powerful approach, aiming to determine the best sea state that explains the observed ship motions. These techniques work by minimizing the discrepancy between the modeled ship response and the actual observations, leading to more accurate sea state estimations (Pascoal et al., 2017; Ren et al., 2021a; Zhang et al., 2024).

The data-driven WBA endeavors to estimate wave information through the utilization of either online or offline training models, aiming to reduce reliance on the RAOs. Therefore, it is crucial to consider well-prepared training data that encompasses a wide range of possible parameter combinations and wave spectrum shapes (Nielsen et al., 2024). Classifiers (Tu et al., 2018), convolutional neural networks (Cheng et al., 2019; Kawai et al., 2021), adversarial networks (Han et al., 2022b), and multi-task learning (Mittendorf et al., 2022) techniques are often employed to capture the complexity of sea state estimation. A comparison between time-domain and frequency-domain models in terms of accuracy is essential to evaluate their performance (Mittendorf et al., 2022). Additionally, the involvement of physics-based information can significantly improve accuracy by integrating model-based wave-ship interactions into the learning framework (Han et al., 2022a; Nielsen et al., 2023b). Nevertheless, the constraints imposed by the scarcity of training data and the high computational costs must be taken into account.

Aside from sea state estimation, there are also intriguing topics and research within the WBA framework. The investigation of parameterized, frequency-domain models using alternative inputs like hull stress responses represents a key effort to further utilize monitoring data (Chen et al., 2021, 2020). Concurrently, advancing high-resolution, phase-resolved wave reconstruction in the time-domain is essential for handling short-term and multi-directional sea states (Takami et al., 2022, 2023). Identifying or tuning a ship seakeeping model parameters is one such topic (Takami et al., 2024; Han et al., 2021; Brodtkorb and Nielsen, 2023). Additionally, multi-spectral fusion techniques have been explored to improve sea state estimation (Nielsen et al., 2019; Zhang and Ren, 2025). Furthermore, addressing the correction of the Doppler effect in advancing ships is another important consideration in this field (Nielsen, 2017; Mounet et al., 2023).

Estimating the wave spectrum requires time-frequency transformation, a crucial preliminary step in converting time-domain responses into the frequency domain. For wave rider buoys, the power spectral density of heave, pitch, and roll motions can be directly used to derive wave parameters. In large-scale observations, time-involved sea conditions are often simplified to a stationary system, allowing for 30-min manual segmentation in moored buoy measurements, a practice also common in WBA. However, such simplifications introduce inaccuracies and uncertainties in onsite WBA operations by neglecting time-dependent variations. Additionally, small deviations in the response spectra can be significantly amplified in the ill-posed system, leading to potentially misleading estimates.

To address these challenges, we propose a wavelet-based adaptive segmentation algorithm that enhances real-time WBA performance by adapting to time-involved sea states. Simulations verify the method's effectiveness in capturing the inherent variability of ocean waves. The main contributions of the present study are highlighted as follows

- Semi-stationary evolutionary sea states are considered to closely reflect practical sea conditions.
- Wavelet-based response spectral analysis is applied for balancing time-domain resolution and frequency-domain accuracy.
- Adaptive segmentation algorithm is introduced to detect the evolution in the time-involved sea state, enhancing real-time capabilities.

The paper is organized as follows. Section 2 formulates the WBA problem within a mathematical framework and outlines the challenges this work aims to address. Section 3 introduces the proposed adaptive segmentation algorithm. Section 4 exhibits the simulation results and Section 5 concludes the study.

2. Problem formulation

2.1. Ship as a buoy

The conception of using an oscillating ship as a wave buoy to observe the real-time sea state is building upon the simplified linear relationship between waves and ship responses. The wave-induced forces and moments acting on the ship are typically determined using potential flow theory, assuming inviscid, incompressible, and irrotational flow. Within a simplified framework of wave-body interaction, the ship's motions are assumed to be small and proportional to the wave amplitudes, allowing for a linear superposition of wave-induced responses in the time domain. Meanwhile, in the frequency domain, the motion RAOs describe how a ship responds to wave excitation at different frequencies, thus establishing a connection between the wave spectrum and the ship's motion spectra. The WBA involves the inverse resolution of wave information by leveraging easily accessed ship motions (see Fig. 1).

In this study, the dynamic positioning (DP) scenario, a common situation in marine operations, is considered. The global reference frame is oriented with true north at zero degrees, progressing clockwise, and the distribution along a ship's longitudinal axis is referred to as the body-fixed reference frame. The ship's six degrees of freedom (DOFs) motions (surge, sway, heave, roll, pitch, yaw) are indexed by the set $\mathbb{J} = \{1, 2, 3, 4, 5, 6\}$, respectively. Heave, roll, and pitch motions are utilized to derive real-time sea state because the influence of the DP system can be neglected (Skjetne and Ren, 2020), i.e., $\mathbb{I} = \{3, 4, 5\} \subseteq \mathbb{J}$. The total number of selected motions is denoted by $N_d = 3$. The directional wave spectrum, denoted by $E(\omega, \alpha)$, is a two-dimensional variable that varies with frequency ω and incoming wave direction α. During onsite observation, the ship's heading angle with respect to the true North, denoted by η, is known and used to transform from body-fixed to global references frame. The transformation is represented as $E(\cdot, \beta) = E(\cdot, \alpha - \eta)$, where β is the wave direction relative to the vessel's heading (see Fig. 2).

The linear wave-ship system in the frequency domain is discretized into a network with N_ω frequencies and N_β directions. The specific frequency and direction are indexed by $m \in \mathbb{M} = \{1, \cdot s, N_\omega\}$ and $n \in \mathbb{N} = \{1, \cdot s, N_\beta\}$, respectively. Consequently, the ship's response cross-spectra at specific frequency ω_m can be expressed as the integral over all wave headings, yielding

$$\begin{aligned} S_{ij}(\omega_m) &= \int_{-\pi}^{\pi} \Phi_i(\omega_m, \beta)\overline{\Phi_j(\omega_m, \beta)}E(\omega_m, \beta)\,\mathrm{d}\beta \\ &\approx \Delta\beta \sum_{n=1}^{N_\beta} \Phi_i(\omega, \beta_n)\overline{\Phi_j(\omega_m, \beta_n)}E(\omega_m, \beta_n), \end{aligned} \tag{1}$$

where S_{ij} is the cross-spectra between the ith and jth DOFs with $i, j \in \mathbb{I}$, Φ is the complex transfer function $\Phi(\omega, \beta) = \Re(\Phi(\omega, \beta)) + \mathbf{i}\Im(\Phi(\omega, \beta))$, and $\Delta\beta$ is the intervals among the discrete β_n. Because of the complex

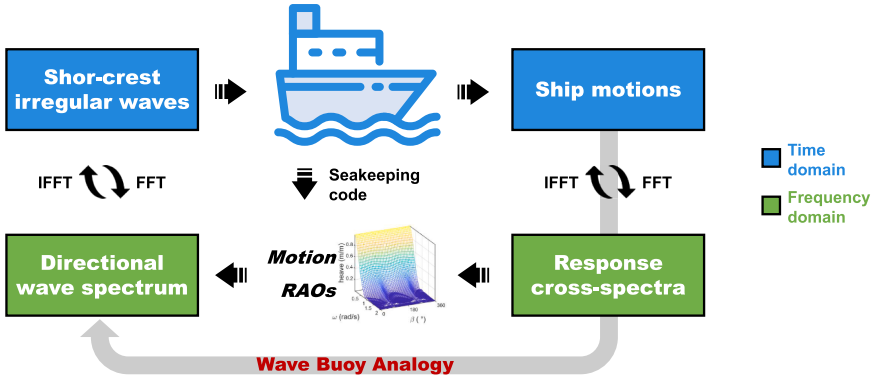

Fig. 1. Overview of the WBA concept.

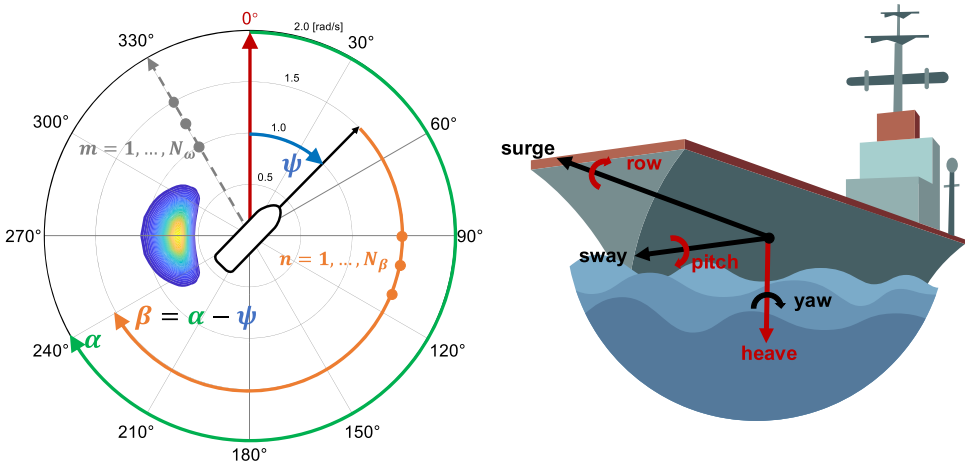

Fig. 2. Ship's coordinate system and the the six degrees of freedom.

nature of cross spectra and transfer functions, the linear equation Eq. (1) at specific frequency can be formulated in a three-section vector form, expressed as

$$b_m = A_m f_m \tag{2}$$

where $b_m \in \mathbb{R}^{N_d^2}$ is a vector containing elements related to the real and imaginary parts of the response spectra, $A_m \in \mathbb{R}^{N_d^2 \times N_\beta}$ is a three-section matrix constructed from transfer functions, and $f_m \in \mathbb{R}^{N_\beta}$ involves the wave spectrum at specific frequency, given by

$$b_m(\omega_m) = \left[S_{ii}(\omega_m), \ldots, \Re(S_{ij}(\omega_m)), \ldots, \Im(S_{ij}(\omega_m)), \ldots\right]^\top, \tag{3a}$$

$$A_m(\omega_m) = \begin{bmatrix} \cdot s & \Re(\Phi_i(\omega_m,\beta))\Re(\Phi_i(\omega_m,\beta)) + \Im(\Phi_i(\omega_m,\beta))\Im(\Phi_i(\omega_m,\beta)) & \cdot s \\ \vdots & & \\ \cdot s & \Re(\Phi_i(\omega_m,\beta))\Re(\Phi_j(\omega_m,\beta)) + \Im(\Phi_i(\omega_m,\beta))\Im(\Phi_j(\omega_m,\beta)) & \cdot s \\ \vdots & & \\ \cdot s & \Im(\Phi_i(\omega_m,\beta))\Re(\Phi_j(\omega_m,\beta)) - \Re(\Phi_i(\omega_m,\beta))\Im(\Phi_j(\omega_m,\beta)) & \cdot s \end{bmatrix} \Delta\beta, \tag{3b}$$

$$f_m(\omega_m) = \left[E(\omega_m,\beta_1), E(\omega_m,\beta_2), \ldots, E\left(\omega_m,\beta_{N_\beta}\right)\right]^\top. \tag{3c}$$

Assembling equations from all considered frequencies yields

$$\mathbf{b} = \mathbf{A}\mathbf{f}, \tag{4}$$

where $\mathbf{b} = [b_1^\top, b_2^\top, \ldots, b_{N_\omega}^\top]^\top \in \mathbb{R}^{N_d^2 N_\omega}$, $\mathbf{A} \in \mathbb{R}^{N_d^2 N_\omega \times N_\beta N_\omega}$, and $\mathbf{f} = [f_1^\top, f_2^\top, \ldots, f_{N_\omega}^\top]^\top \in \mathbb{R}^{N_\beta N_\omega}$. The cutoff frequency ω_{N_ω} is selected where the values of the response spectra tend towards zero, which means the wave-induced responses excited by the wave components with frequencies larger than ω_{N_ω} are neglected. Hereafter, the sea state estimation involves solving for the unknown directional wave spectrum from Eq. (4), which is an ill-posed inverse problem.

One commonly used technique for addressing inverse problem is convex optimization. Sparse regression can be introduced to improve the estimation performance. The sparsity and smoothness control terms for wave spectrum estimation have been described in previous study (Ren et al., 2021a). Regularization regression based cost function is established to calculate the vector-form wave spectrum $\mathbf{f}$ from the transfer matrix $\mathbf{A}$ and response spectra $\mathbf{b}$, additionally. The wave spectrum estimate $\hat{\mathbf{f}}$ is received by solving the following cost function

$$\begin{aligned} \hat{\mathbf{f}} = \arg \quad & \min_{\mathbf{f}} \ ||\mathbf{A}\mathbf{f} - \mathbf{b}||_2^2 + \gamma_1 ||\mathbf{f}||_1 + \gamma_2 ||D\mathbf{f}||_2^2, \\ \text{s.t.} \quad & \mathbf{f} \geq 0, \end{aligned} \tag{5}$$

where γ_1 and γ_2 are tuning parameters that provide trade-offs between accuracy and smoothness. The matrix D is a differential matrix specifically constructed to enforce this smoothness. It is built as a sparse matrix, with its rows designed to calculate the second-order differences between adjacent elements of the $\mathbf{f}$ vector. This calculation is performed along both the frequency (ω) and directional (β) dimensions of the wave spectrum. Therefore, minimizing the $||D\mathbf{f}||_2^2$ term "penalizes" any solution $\hat{\mathbf{f}}$ that is not smooth, i.e., has high curvature or sharp oscillations, ensuring unsmooth estimates are less likely to be accepted. Since the real wave spectrum is non-negative, the constraint $\mathbf{f} \geq 0$ is enforced in Eq. (5). Finally, by reshaping the optimal $\hat{\mathbf{f}}$ into a matrix, we obtain the estimated directional wave spectrum, representing the current sea state.

2.2. Semi-stationary wave-ship interaction

Ocean waves are inherently non-stationary processes, with properties that change constantly over time. Consequently, wave-induced responses in floating structures exhibit time-dependent variability, as their transfer functions are generally time-invariant. A stationary assumption

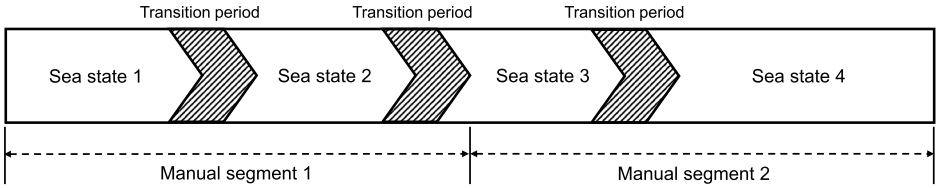

Fig. 3. Construction of the semi-stationary sea states.

is often applied in large-scale observational analysis to facilitate statistical estimation (Iseki and Ohtsu, 2000). However, the simplification is not suitable for capturing the short-term, time-dependent variation that is crucial for WBA techniques.

time-involved sea states are modeled to demonstrate the necessity and effectiveness of the proposed method. An approach termed 'semi-stationary sea states' is introduced, defined as an evolutionary process where wave properties change continuously. Such a definition contrasts with earlier approaches that assumed constant half-hour intervals.

The simulation of this evolutionary process is inspired by configurations in marine operation software (SINTEF, 2024). A one-hour condition is divided into four sequential stages, with the specific time of each changepoint occurring randomly. To model a continuous, non-discrete evolution, 'evolutionary phases' are introduced between the stages. During these phases, the wave parameters undergo a linear interpolation from the preceding stage's parameters to the next. This combination of random changepoints and gradual, linear evolution is intended to approximate the unpredictable and continuous nature of real-world sea states. The resulting model structure is illustrated in Fig. 3 and represents a continuous process.

The semi-stationary wave spectrum with time-involved wave parameters can be established as

$$E(\omega,\beta,t) = P(\omega,t) \cdot pN(\beta,t). \tag{6}$$

In the construction of the semi-stationary directional wave spectrum $E(\omega,\beta,t)$, the time dependent wave spectrum $P(\omega,t)$ and spreading function $N(\beta,t)$ are cross-multiplied.

The wave spectrum was discretized into a $N_\omega \times N_\beta$ matrix. The transfer functions for wave-response interaction were discretized on the same scale. The responses of the DP ship under such a semi-stationary sea state can be modeled as a superposition of the product of the RAOs and the directional wave spectrum, which encompasses all wave frequencies and directions, given by

$$R_i(t) = \sum_{m=1}^{N_\omega}\sum_{n=1}^{N_\beta} a_{mn}(t)\cos(\omega_m t + \phi_{mn} + \epsilon_{mn}), \tag{7a}$$

$$a_{mn}(t) = |\Phi_i(\omega_m,\beta_n)|\sqrt{2E(\omega_m,\beta_n,t)\Delta\omega\Delta\beta}, \tag{7b}$$

$$\phi_{mn} = \arctan\left(\frac{\Im[\Phi_i(\omega_m,\beta_n)]}{\Re[\Phi_i(\omega_m,\beta_n)]}\right), \tag{7c}$$

where R_i denote the ship's motion at specific DoF, ϕ_{mn} represents the phase information of the ship motion RAO, and ϵ_{mn} represents the random phase of the waves at specific frequency ω_m and wave heading β_n. Total number of N_ω frequencies and N_β wave directions are considered. The increments of the discrete frequencies and directions are denoted as $\Delta\omega$ and $\Delta\beta$ respectively.

2.3. Necessity of time-involved analysis

The assumption of stationary sea conditions, commonly approximated by 30-min segmentation, is widely adopted within the WBA community for near real-time measurements (Nielsen and Dietz, 2020; Han et al., 2022b). While this approach may be suitable for long-term analyses, such as seasonal or annual forecasting with fixed-position wave rider buoys, short-term variations in wave direction and frequency are critical for supporting onsite marine operations, where specific wave characteristics can significantly impact activities. Unlike wave buoys, which allow direct derivation of sea states through power spectral density analysis, WBA faces a highly ill-posed inverse wave spectrum resolution problem, where even minor biases in the cross-spectra of ship responses can result in considerable errors in wave spectrum estimates.

Based on Eq. (4), a theoretical benchmark can be established for the input to the WBA solver. We define this as the ideal response spectra: the spectra derived directly from the mathematical model by multiplying the known transfer functions with the ground truth semi-stationary wave spectra. Fig. 4 illustrates the time-frequency distributions of these ideal self and cross spectra for a predefined semi-stationary sea state. The specific case shown is Sea state 1. The detailed formulation of which is presented in Section 4.3 and Table A.1. As the figure highlights, even with narrow changes in the input wave parameters, the ideal response spectra exhibit significant variations.

In such semi-stationary conditions, the traditional segmentation–defined here as the common practice of applying a fixed 30-min window to the data–introduces significant uncertainties. The traditional approach incorrectly averages across distinct, evolving sea states. The uncertainty complicates WBA efforts to achieve stable and reliable sea state estimation, as the ill-posed nature of the problem leads to a lack of unique solutions and heightened sensitivity to perturbations. Deviations in the spectral analysis of ship motions can evolve into significant errors in sea state estimates.

To demonstrate the necessity of time-involved response spectral analysis, a comparative case study was conducted. This study utilizes a 60-min simulation of a semi-stationary sea state, which is composed of four sequential stages connected by gradual transitions. For this comparison, Stage 4 from Sea state 1 was selected, as detailed in Table A.1 As illustrated in Fig. 5, four distinct estimations for this specific stage are presented for comparison:

- Preset spectrum: This represents the ground truth, predefined directional wave spectrum for the selected stage as defined by the simulation parameters.
- Estimate from ideal response spectra: This represents a theoretical benchmark, corresponding to the WBA solver's output when provided with the perfect, analytically derived response spectra.
- Estimate from corresponding section: This represents an idealized benchmark. It is the estimate derived from the time-series data using only the correct time window. This demonstrates the potential WBA performance under conditions of perfect temporal segmentation.
- Estimate from 30-min Section: This represents the traditional, non-adaptive method. It is the estimate derived from a fixed 30-min window, which incorrectly averages the temporal data.

It can be observed that the WBA framework achieves highly accurate estimates when provided with ideal response spectra. When using the correct time window segmentation corresponding to the semi-stationary wave stage, the main characteristics of the waves are accurately captured. However, when adopting the traditional 30-min segmentation strategy, the results show significant deviations, highlighting the system's sensitivity to inaccuracies in the input data.

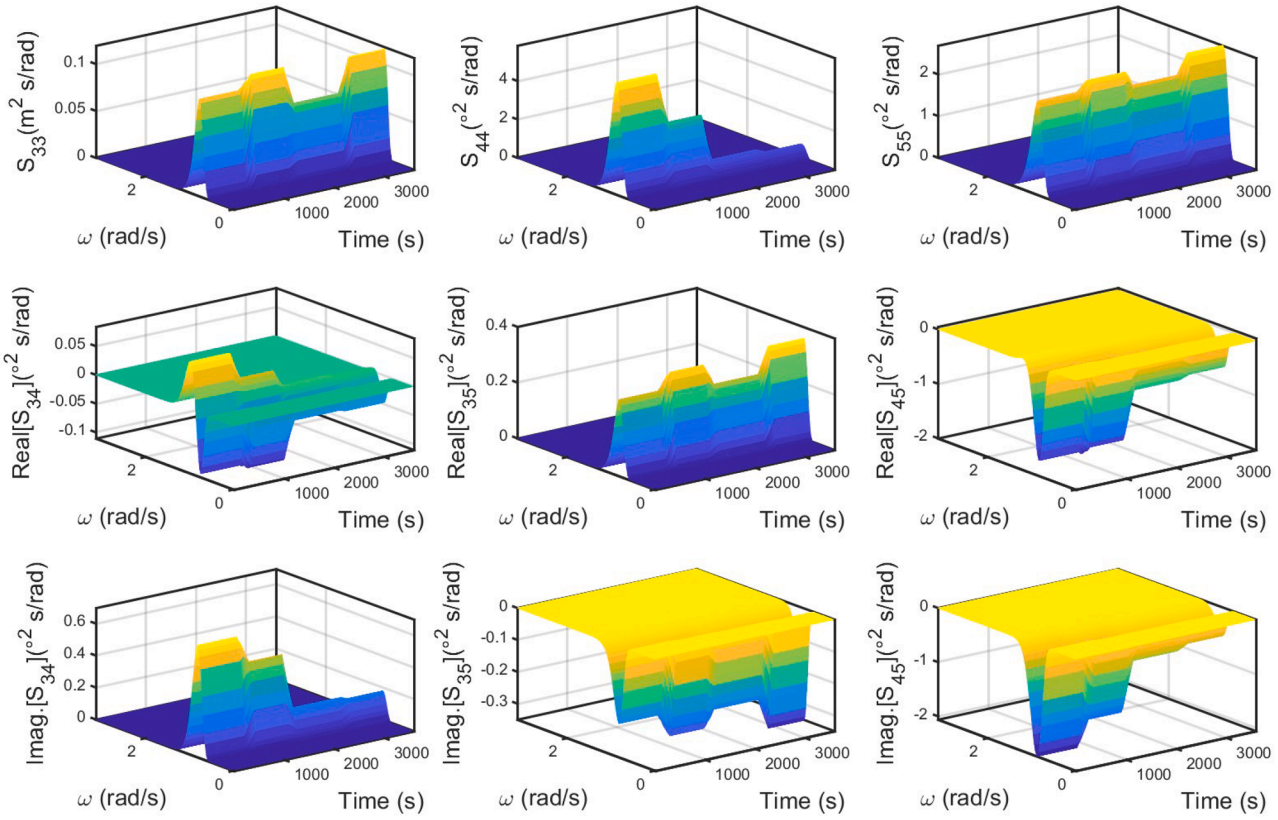

Fig. 4. Response spectra under the semi-stationary sea states.

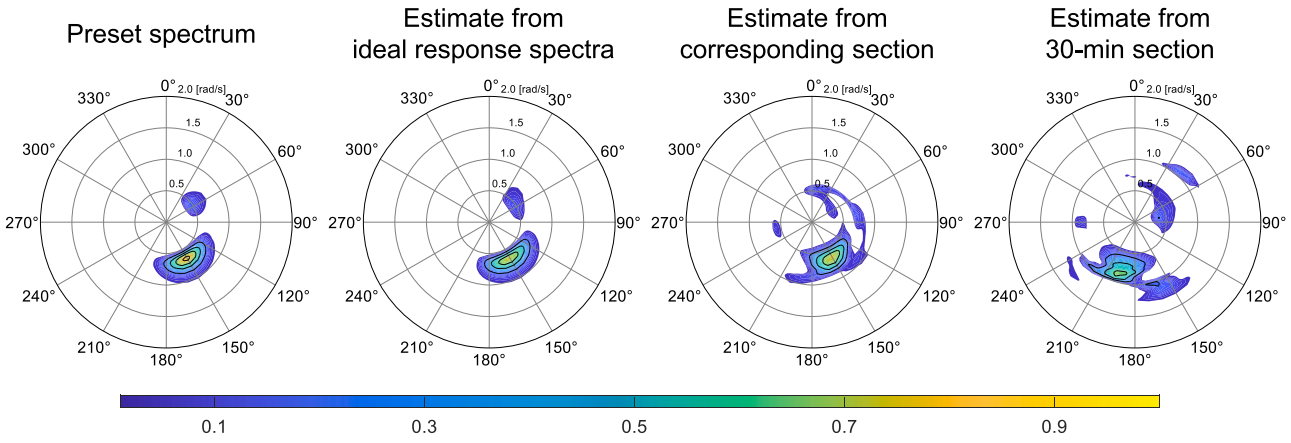

Fig. 5. Estimates of semi-stationary sea states using input response spectra in different time windows.

This clearly demonstrates the inadequacy of a fixed-segmentation approach. Real-world sea states are not truly stationary but are characterized by a random, non-stationary evolution. This inherent stochasticity introduces significant uncertainty into the response spectral analysis. Given that the WBA framework is a highly ill-posed inverse problem, any such spectral uncertainties are prone to significant amplification, leading to large and potentially misleading estimation errors. It is therefore crucial to develop a robust methodology capable of identifying and accounting for these random temporal variations in the ship's response, effectively balancing the inherent time-frequency trade-off to capture the evolving sea state characteristics.

2.4. Problem statement

In this study, the application of the WBA is extended to time-dependent sea state estimation by accounting for semi-stationary waves. However, traditional response signal processing methods are inadequate, as they assume stationarity, overlook the inherently time-involved nature of waves, and introduce misleading errors in estimates. To capture time-involved variations, time-involved response spectral analysis is essential for balancing time-domain resolution and frequency-domain accuracy, providing accurate and robust input for the WBA and enabling more reliable and responsive wave spectrum estimations.

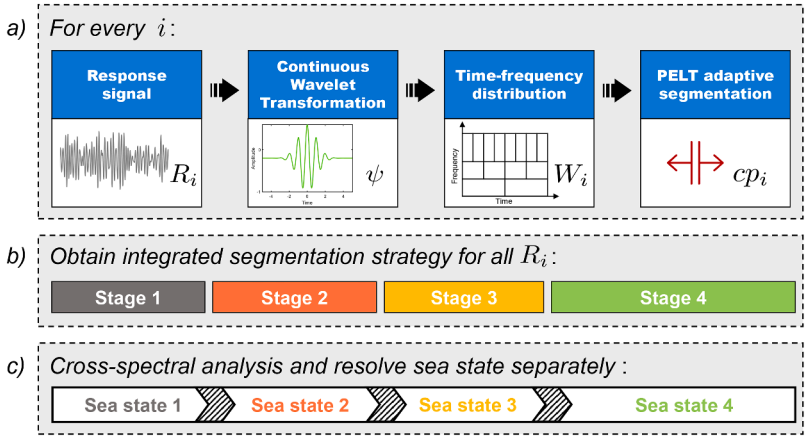

Fig. 6. Application procedure of the wavelet-based adaptive segmentation method.

3. Wavelet-based adaptive segmentation

In spectral analysis, the time-frequency resolution requires a trade-off, referring to the inherent compromise between time and frequency resolution when analyzing signals that vary over time, particularly in non-stationary processes. The trade-off arises from the uncertainty principle in signal processing, which states that it is impossible to simultaneously achieve high precision in both time and frequency domains. In this section, a wavelet-based time-frequency analysis is proposed to support adaptive time series segmentation, enabling more accurate detection of time-involved characteristics in the sea waves.

3.1. Wavelet-based time-frequency analysis

Ocean waves exhibit unique time-frequency characteristics, marked by their low-frequency oscillations and complex energy distribution patterns. Unlike high-frequency signals, which display rapid variations and sharp peaks, ocean waves evolve more gradually over time. As a result, commonly used time-frequency analysis methods, such as those applied in areas like voice, earthquake, and electroencephalogram signal analysis, encounter challenges when adapted to the slower, more complex dynamics of floating structure behavior (Newman, 2018).

The wavelet transform is a potent mathematical technique used to process and analyze signals, enabling the decomposition of a signal into different scale or resolution components. In contrast to the Fourier transform's breakdown of a signal into sine and cosine functions with varying frequencies, the wavelet transform employs wavelets (small oscillations resembling waves) that are localized in both time and frequency domain (Sifuzzaman, 2009). The wavelet transform's ability to localize signals is particularly advantageous for analyzing time-involved and non-stationary signals with dynamic frequency characteristics. Unlike the short-time Fourier transform (STFT), which operates with a fixed window size, the wavelet transform adapts its window size based on the frequency being analyzed narrowing for high frequencies and widening for low frequencies. This adaptive feature enhances the frequency resolution for low-frequency components, capturing subtle variations in longer waves, while improving the time resolution for high-frequency components, where rapid changes occur. As a result, the wavelet transform provides a more flexible and detailed analysis across a wide range of frequency bands.

The mathematical representation of the continuous wavelet transform (CWT) can be expressed as follows

$$W_i(a,b) = \int_{-\infty}^{\infty} R_i(t)\psi_{a,b}(t)dt \tag{8a}$$

$$\psi_{a,b}(t) = \frac{1}{\sqrt{|a|}}\psi\left(\frac{t-b}{a}\right) \tag{8b}$$

where $\psi_{a,b}(t)$ is the scaled and translated wavelet function, a and b is the scaling parameter and the translation parameter respectively. In the current study, the Morlet wavelet function is used as the basis function, expressed as

$$\psi(t) = \frac{1}{\sqrt{\pi\sigma}} e^{\mathbf{i}\omega_0 t} e^{-\frac{t^2}{2\sigma^2}} \tag{9}$$

where ω_0 is the central frequency of the wavelet, σ is the standard deviation, and $\mathbf{i}$ is the imaginary unit. After applying the wavelet transform to the ship's response signals, which are excited by time-involved sea states, a two-dimensional time-frequency power distribution is obtained.

3.2. Adaptive segmentation by PELT algorithm

By applying the CWT, the time-frequency power distribution of ship motions can be obtained, revealing how different frequency components evolve over time. However, further segmentation is needed to accurately identify and capture changes in the sea state. The pruned exact linear time (PELT) (Killick et al., 2012) method is a statistical approach used to identify change points within time series data, with the goal of achieving precise, optimal segmentation. The method begins by defining a cost function for segmenting the time series and initializing a set of candidate change points. Next, PELT computes the cost of segmenting the series up to each candidate point and incorporates the cost of the segment that follows the change point. A pruning condition is then applied to discard candidate points that cannot improve the current best solution. This iterative process continues until all points have been evaluated, ensuring that the remaining candidates represent the minimal cost segmentation of the time series. By traversing all considered motion DoFs, an integrated change points set can be obtained. The pseudo-code for PELT is shown in Algorithm 1.

By minimizing the overall cost of segmentation, the PELT incorporates a penalty term β to prevent overfitting by penalizing the introduction of unnecessary changepoints. The mean and variance are selected as the statistics to measure the fit condition of candidate changepoints. The fit measure function C for the two-dimensional wavelet matrix is given by

$$C\left(W_{i\,[(\tau+1):\tau^*)]}\right) = \sum_{a=1}^{N_a}\sum_{t=\tau+1}^{\tau^*}\left(W_i(a,t) - \text{mean}\left(W_i\left(a,\left[(\tau+1):\tau^*\right]\right)\right)\right)^2. \tag{10}$$

The process begins with initializing key variables and then iteratively calculating the optimal cost for each potential change point by considering previous candidates and updating the set of potential change

points through a pruning mechanism. The pruning step, based on a constant K, ensures computational efficiency by discarding less promising candidates.

The PELT algorithm not only identifies the change points based on different penalty parameter β but also allows for flexibility by setting parameters such as the desired number of change points or the minimum segment length. This flexibility makes PELT highly adaptable to different applications. In the context of WBA, the algorithm can be adjusted according to the specific needs of the operation, ensuring that it provides the required segmentation for real-time monitoring.

3.3. Workflow for adaptive segmentation

The adaptive segmentation process significantly enhances cross-spectral analysis of ship responses, improving accuracy while accommodating time-domain variations. The workflow is illustrated in Fig. 6. Initially, ship responses for the relevant DOFs are collected, followed by the CWT to obtain the time-frequency power distribution. The PELT algorithm is then applied to the wavelet matrices to identify optimal segmentation points. Typically, change points across different DOFs are similar. However, under specific sea states, such as head seas, the roll motion may be minimal, making it difficult to detect sea state changes using only the roll motions as an input. Therefore, incorporating all DOFs improves the robustness of the proposed adaptive segmentation approach and results in an integrated segmentation strategy. After adaptive segmentation, sea states at different stages can be estimated through cross-spectral analysis of ship motion, with each stage analyzed individually. Subsequent experiments will validate the performance advantages of the proposed method compared to traditional direct segmentation.

Algorithm 1 PELT algorithm.

Input: Wavelet matrix $W_i(a,t)$ at DoF i, cost function that measures the fit of segments between change points $C(.)$, penalty parameter β, constant for pruning K.
Output: {cp}, integrated change points set.
Initialize:
$F(0) \leftarrow -\beta$; ▷ *Negative cost to account for no change points initially*
cp(0) ← Null; ▷ *No change points at the start*
$R_1 \leftarrow \{0\}$. ▷ *Initialize the set of candidate change points with only 0*
Body:
for $i = 1:\ N_d$ **do** ▷ *Traverse all considered DoFs*
  for $\tau^* \leftarrow 1:$ length(W) **do** ▷ *Iterate over each time point*
    $F(\tau^*) \leftarrow \min_{\tau \in R_{\tau^*}} \left[F(\tau) + C(W_{i\,[(\tau+1):\tau^*)]}) + \beta\right]$ ▷ *Compute the minimum cost*
    $\tau_{\text{opt}} \leftarrow \arg\min_{\tau \in R_{\tau^*}} \left[F(\tau) + C(W_{i\,[(\tau+1):\tau^*)]}) + \beta\right]$ ▷ *Identify optimum candidate*
    $\text{cp}_i(\tau^*) \leftarrow [\text{cp}_i(\tau_{\text{opt}}), \tau_{\text{opt}}]$ ▷ *Update the list of change points*
    $R_{\tau^*+1} \leftarrow \left\{\tau \in R_{\tau^*} \cup \{\tau^*\} : F(\tau) + C(W_{i\,[(\tau+1):\tau^*)]}) + K \le F(\tau^*)\right\}$ ▷ *Prune the candidate set for the next iteration*
  end for
end for
Post-processing:
$\{\text{cp}\} \leftarrow \text{sort}(\bigcup_{i=1}^{N_d} \text{cp}_i)$ ▷ *Combine and sort change points across DoFs*
for $j = 2$ **to** length(cp) **do**
  if $\text{cp}(j) - \text{cp}(j-1) < \delta$ **then**
    $\{\text{cp}\} \leftarrow \{\text{cp}\} \setminus \{\text{cp}(j)\}$ ▷ *Remove duplicates from the set*
  end if
end for
  return {cp}

4. Simulation results

4.1. Simulation setup

Numerical simulations were conducted to demonstrate the efficiency of the proposed adaptive segmentation strategy. Semi-stationary sea states were modeled over a 60-min period to demonstrate the limitations of traditional methods and to highlight the effectiveness of the proposed adaptive segmentation approach. This 60-min period was divided into four sequential stages, with the specific changepoints occurring randomly, connected by three evolutionary phases applying linear interpolation. The two-peak JONSWAP wave spectrum is considered, given by

$$E(\omega,\beta,t) = \sum_{\kappa} P_{\kappa}(\omega,t) \cdot pN_{\kappa}(\beta,t). \tag{11a}$$

$$P_{\kappa}(\omega,t) = \frac{H_{s,\kappa}^2 \left[\left(\frac{4\lambda+1}{4}\right)(\omega_{p,\kappa}(t))^4\right]^{\lambda}}{4\Gamma(\lambda)\omega^{4\lambda+1}} \exp\left[-\frac{4\lambda+1}{4}\left(\frac{\omega_{p,\kappa}(t)}{\omega}\right)^4\right], \tag{11b}$$

$$N_{\kappa}(\beta,t) = \frac{2^{2s_{\kappa}-1}\Gamma^2(s_{\kappa}+1)}{\pi\Gamma(2s_{\kappa}+1)} \cos^{2s_{\kappa}}\left(\frac{\beta-\beta_{p,\kappa}(t)}{2}\right). \tag{11c}$$

Here, $\kappa = 2$ indicates the presence of two distinct spectral peaks, representing wind waves and swell waves separately. H_s is the significant wave height, ω_p is the peak angular frequency, β_p is the mean wave direction, Γ is the Gamma function, and s and λ are the shape parameters. The dominating wave parameters, such as significant wave height $H_s(t)$, peak wave frequency $\omega_p(t)$, and mean wave direction $\beta_p(t)$ within each stage fluctuate in a reasonable range, ensuring the time-involved characteristic of the semi-stationary process and avoiding sudden, unreasonable changes.

Moderate sea states were applied, as WBA techniques are better suited to the linear wave assumption in such conditions, which are also more commonly observed. Series of time-involved sea states were established, with significant wave heights H_s ranging from 0.3 to 2 m, wave periods T_p between 5 and 15 s, and wave directions β_p randomly distributed from 0 to 360°. Wind waves were set as the dominant term, characterized by higher wave heights, longer wave periods, and a more scattered energy distribution, such that $H_{s,1} > H_{s,2}$, $T_{p,1} > T_{p,2}$, and $s_1 < s_2$. All considered sea state are listed in Table A.1.

A key parameter in the adaptive segmentation is the penalty term, β, used by the PELT algorithm, which controls the sensitivity of the changepoint detection. In the simulations presented, the semi-stationary process is idealized with relatively distinct evolutionary phases, the segmentation results were not highly sensitive to the precise value of β. However, the parameter's role is critical in real-world applications where sea state evolution is more complex and the ground truth is unknown. In such operational scenarios, β serves as a tunable parameter. It can be adjusted by the operator based on specific needs, such as setting a high value to capture only large-scale, significant changes or a lower value to detect more subtle, frequent variations.

4.2. Sea states change points identification

A cargo ship with a length of 55 m, a breadth of 12 m, and a draught of 4 m was used, and the RAOs, or transfer functions, were calculated using seakeeping code, as illustrated in Fig. B.1. Sea state 1 is selected as an example to demonstrate the procedure of the proposed algorithm.

The generated ship motions under Sea state no.1 are presented in Fig. 7, illustrating the heave, roll, and pitch motions. Wavelet transformation was applied to analyze the time-frequency power distribution of the ship responses, followed by the implementation of the PELT algorithm to detect change points in the time-involved sea state.

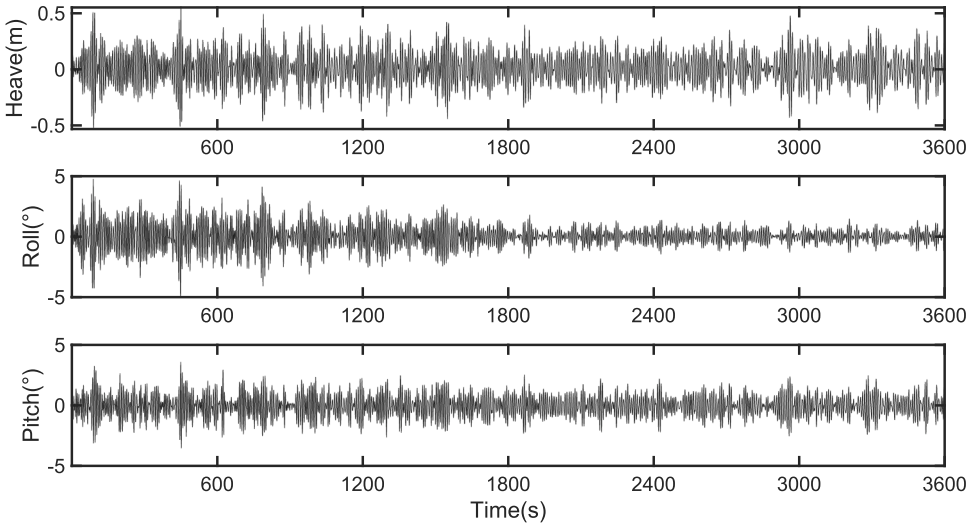

Fig. 7. Heave, roll, and pitch motions.

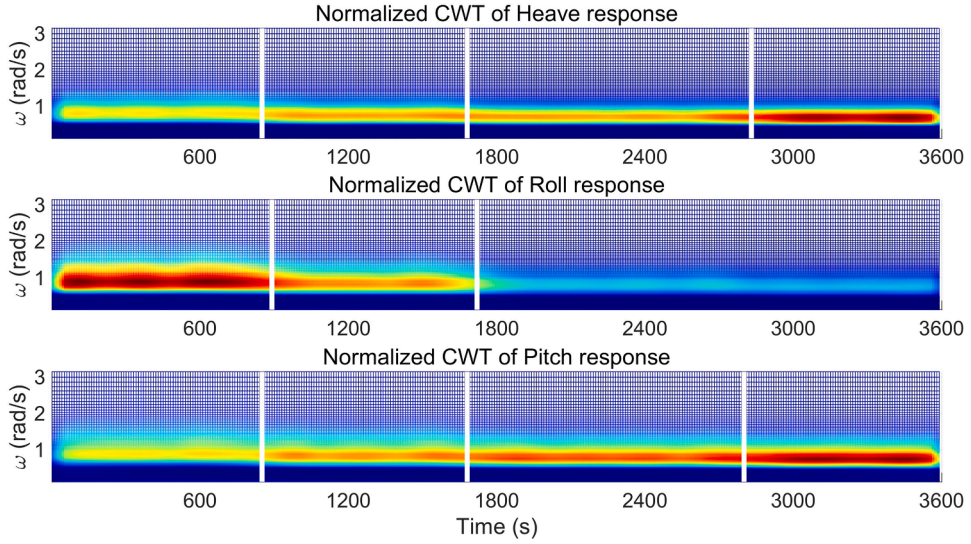

Fig. 8. Normalized CWT result of simulated ship responses, with gaps indicating detected change points using the PELT algorithm.

The resulting normalized time-frequency power distributions are shown in Fig. 8, where colors from blue to red represent low to high power, respectively (on a scale from 0 to 1). The change points identified by the PELT algorithm are marked by vertical gaps. It is evident that the detected change points across different motion responses generally fall within a similar range. However, in some specific conditions, such as the case study depicted in Fig. 8, the roll motion misses a change point that the heave and pitch motions detect at around 2700 second. By considering the change points from the three degrees of freedom collectively, an integrated adaptive segmentation strategy can be developed to enhance time-dependent sea state estimation. Identifying transition periods and adaptively segmenting the data allows regression optimization, following Eq. (5), to derive estimates for each stage.

4.3. Estimates of semi-stationary sea states

A total of 10 predefined semi-stationary sea states were considered, as listed in Table A.1. The preset wave spectrum and wave estimates from different segmentation strategies, 30-min manual separation and the proposed adaptive segmentation approach, were compared using mean square error as an indicator. Response spectral analysis results were also compared with the ideal response spectra, obtained by superposing the preset wave spectra and known transfer functions, to demonstrate the efficiency of the proposed algorithm. In all predefined conditions, the segmentation algorithm successfully detected the change points. The signal processing significantly improved the quality of response spectral analysis and, consequently, provided sea state estimation with lower errors compared to traditional segmentation strategy.

Fig. 9 illustrates the integrated and separated error analysis for both response spectra and sea state estimates under Sea state 1. The integrated error, shown by dashed bars, represents a weighted average result based on temporal weighting. The separated errors indicate the errors at different stages correspond to specific sections within the semi-stationary sea states. The bars above the timeline, in lighter colors, indicate the sea state estimation errors compared to the predefined time-involved sea state. The downward bars represent the response spectra errors relative to the perfect response spectra, displaying the spectral analysis accuracy both integrally and in different stages. Purple and blue represent the traditional 30-min segmentation and the proposed adaptive segmentation, respectively, while black and gray arrows mark the actual and detected change points. It can be observed that under Sea state 1, the change points are correctly

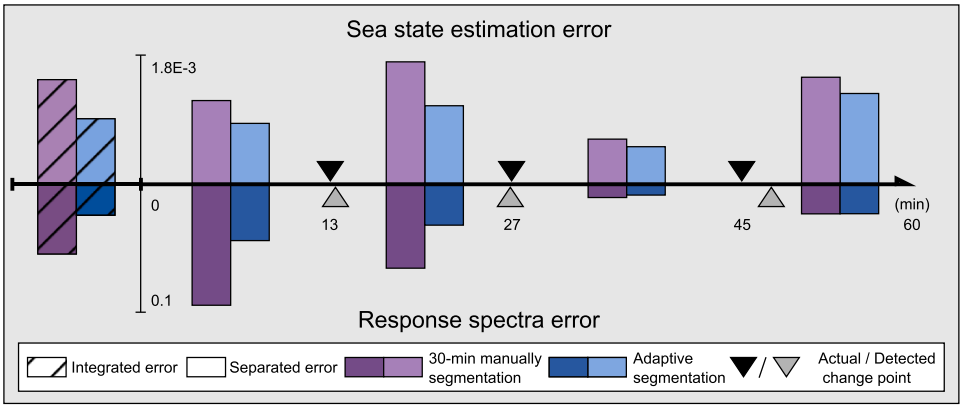

Fig. 9. Error comparison of different segmentation strategies (Sea state 1).

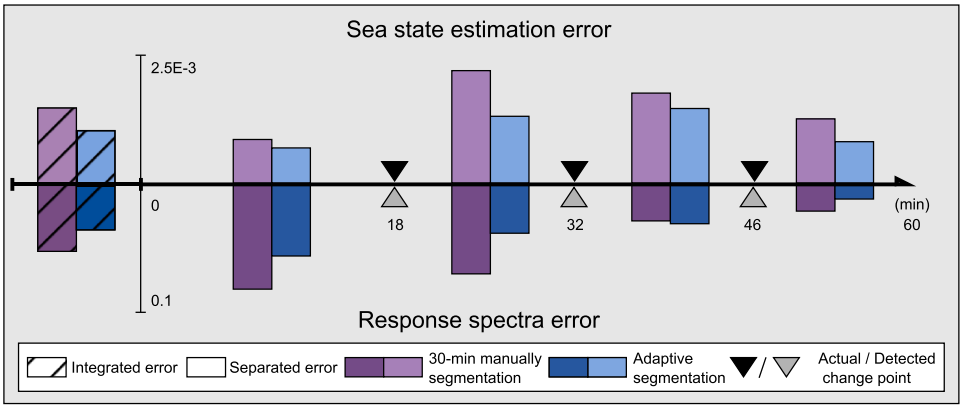

Fig. 10. Error comparison of different segmentation strategies (Sea state 2).

Table 1
Estimate error analysis.

Case	Estimate error analysis (MSE)	Integrated	Stage 1	Stage 2	Stage 3	Stage 4
	Adaptive Seg.	9.05E-04	8.41E-04	1.09E-03	5.14E-04	1.26E-03
1	30-min Seg.	1.45E-03	1.16E-03	1.70E-03	6.20E-04	1.49E-03
	Error reduction rate (%)	37.71	27.53	36.09	17.10	15.32
	Adaptive Seg.	1.03E-03	6.84E-04	1.30E-03	1.45E-03	8.05E-04
2	30-min Seg.	1.49E-03	8.48E-04	2.19E-03	1.77E-03	1.25E-03
	Error reduction rate (%)	43.65	24.00	68.34	22.13	55.08
	Adaptive Seg.	9.39E-04	1.63E-03	5.15E-04	3.60E-04	1.12E-03
3	30-min Seg.	1.36E-03	1.78E-03	1.10E-03	5.57E-04	1.03E-03
	Error reduction rate (%)	31.01	8.16	52.93	35.45	-8.97
	Adaptive Seg.	2.37E-04	2.84E-04	2.13E-04	1.92E-04	2.19E-04
4	30-min Seg.	4.46E-04	1.93E-04	9.12E-04	2.16E-04	5.89E-04
	Error reduction rate (%)	46.84	-46.98	76.60	11.04	62.79
	Adaptive Seg.	1.25E-03	6.73E-04	8.74E-04	1.51E-03	1.65E-03
5	30-min Seg.	2.29E-03	1.44E-03	2.20E-03	3.75E-03	2.18E-03
	Error reduction rate (%)	45.49	53.16	60.34	59.65	24.22
	Adaptive Seg.	5.08E-04	3.58E-04	3.71E-04	6.89E-04	8.70E-04
6	30-min Seg.	7.77E-04	4.40E-04	6.62E-04	8.33E-04	1.46E-03
	Error reduction rate (%)	34.70	18.80	43.94	17.32	40.31
	Adaptive Seg.	9.91E-04	4.64E-04	1.51E-03	8.38E-04	1.54E-03
7	30-min Seg.	2.28E-03	7.36E-04	3.66E-03	1.52E-03	3.69E-03
	Error reduction rate (%)	56.48	36.93	58.85	44.73	58.38
	Adaptive Seg.	4.00E-04	2.04E-04	1.21E-04	9.54E-04	8.81E-04
8	30-min Seg.	4.36E-04	2.05E-04	2.23E-04	1.19E-03	6.94E-04
	Error reduction rate (%)	8.12	0.30	45.80	19.64	-26.98
	Adaptive Seg.	1.04E-03	6.18E-04	4.43E-04	1.50E-03	1.11E-03
9	30-min Seg.	1.90E-03	1.17E-03	6.64E-04	1.59E-03	2.51E-03
	Error reduction rate (%)	45.39	47.04	33.23	5.26	55.73
	Adaptive Seg.	1.38E-03	1.69E-03	1.35E-03	8.03E-04	1.28E-03
10	30-min Seg.	2.04E-03	1.51E-03	2.14E-03	1.62E-03	3.24E-03
	Error reduction rate (%)	32.57	-11.82	37.05	50.32	60.50

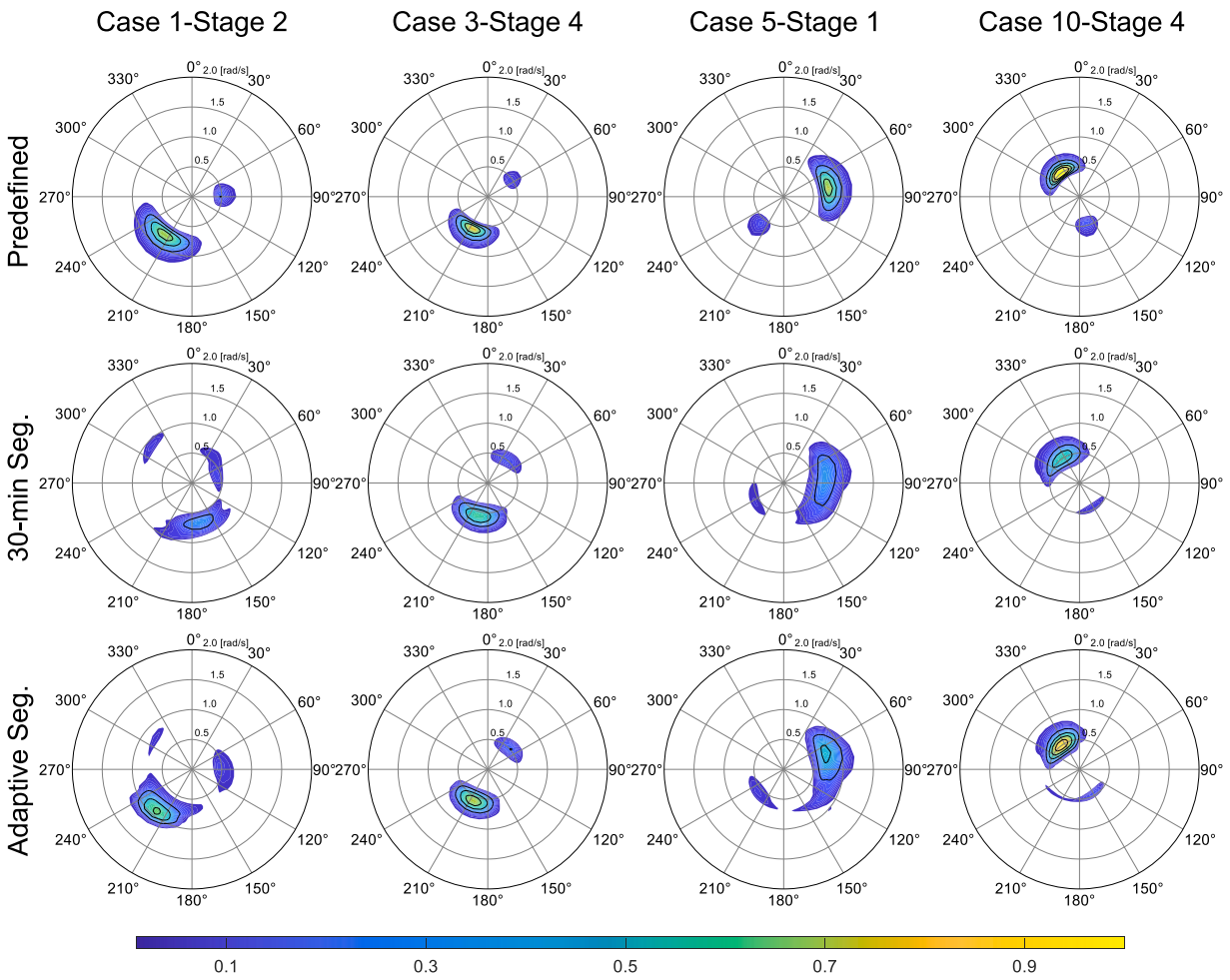

Fig. 11. Typical cases: predefined wave spectrum, estimates from traditional method, and estimates from proposed adaptive segmentation.

identified, and the error indicators consistently demonstrate the advantages of the proposed segmentation algorithm. Additionally, the accuracy of the response spectra is proportional to the accuracy of sea state estimation, highlighting the critical role of data preprocessing in the WBA.

In Fig. 10, for Sea state 2, the change points are accurately detected, and the proposed approach leads to improved estimates. Despite a suboptimal response spectra mean square erro (MSE) in stage 3, the corresponding sea state estimate still achieves a satisfactory result. Additionally, in Table 1, sea state estimation error using the traditional method and the proposed adaptive segmentation for all considered sea states, totaling 40 conditions, are listed. The error reduction rates, expressed as percentages, are analyzed, with blue indicating improved results and red indicating otherwise. It can be observed that across all sea states, the proposed strategy achieves a significantly improved integrated error over time. Specifically, in nearly all 40 conditions, the proposed approach demonstrates lower MSE, with only rare exceptions. These occurrences are attributed to the inherent time-frequency trade-off: the traditional 30-min segment has low variance but high bias, while our adaptive short segment has low bias but higher variance. In these few instances, the higher variance was likely amplified by the ill-posed WBA problem. However, this is an acceptable trade-off, as the method's superior integrated performance across all sea states demonstrates its overall advantage.

Additionally, typical cases are presented in Fig. 11 to demonstrate the errors associated with applying the traditional 30-min segmentation and the improvements achieved by the proposed method. In Case 1, the estimate using 30-min segmentation miscalculated the main wave direction and underestimated the wave energy. When the adaptive segmentation was applied, the estimate improved significantly, and both spectrum peaks are successfully captured. In Case 2, although the traditional method provided a relatively accurate result, there is a slight deviation in the wave direction, and the overall energy is underestimated. The proposed method corrects the deviation. Case 3 represents a distinctive scenario where neither segmentation strategy can achieve an accurate solution. In beam seas, the ship's inherent hydrodynamics limit WBA performance, as discussed in our previous studies (Zhang and Ren, 2025). However, the estimate using adaptive segmentation still achieve better result. In Case 4, the estimate from the 30-min segmentation introduce considerable error by significantly underestimating the wave energy. The proposed method provide a much improved estimation.

5. Discussion

Estimating sea state from ship motions is an indirect observation method that involves response spectral analysis and solving the ill-posed problem arising from complex transfer functions. Accurate estimation in WBA relies heavily on robust response spectra, as the system is highly sensitive to disturbances. Previous studies, which applied a direct segmentation under the assumption of stationarity based on fixed buoy observations, risk introducing inaccuracies. These errors can become further amplified, leading to significant discrepancies in sea state estimation.

In this study, a semi-stationary condition is established, and an adaptive segmentation algorithm is proposed to achieve time-involved estimation. Simulations were conducted to demonstrate the effectiveness of the proposed method in comparison to traditional approach.

It is important to acknowledge the scope of the present study, which in turn highlights clear directions for future research. The simulation study herein, involving semi-stationary sea states, was designed to demonstrate the feasibility and illustrate the mechanism of the proposed algorithm, rather than to serve as an exhaustive statistical analysis. Although the semi-stationary sea state establishment was inspired by commercial software, it may not fully represent the actual complexity of real sea states. Further, the primary assumption was the use of a perfect transfer function (RAO). In practical applications, however, RAO uncertainty remains a critical challenge for all model-based WBA techniques, as non-uniformly distributed RAOs can cause significant performance deterioration and lead to erroneous estimations. We have addressed this specific challenge in our related research (Zhang and Ren, 2025), which introduced the restricted isometry property to evaluate WBA performance. This provides an RAO-driven assessment criterion to assess the reliability of an estimate based solely on the RAO input.

To accurately capture the complex, time-involved characteristics of the physical sea state, further research is crucial, which must be validated against on-site measurement data.

CRediT authorship contribution statement

Taiyu Zhang: Writing – review & editing, Writing – original draft, Visualization, Software, Methodology, Conceptualization; **Can Ma:** Writing – review & editing, Validation, Software, Methodology; **Yang An:** Visualization, Supervision, Methodology, Funding acquisition, Conceptualization; **Zhengru Ren:** Writing – review & editing, Supervision, Resources, Funding acquisition, Conceptualization.

Declaration of competing interest

The authors declare that they have no known competing financial interests or personal relationships that could have appeared to influence the work reported in this paper.

Acknowledgment

This work was supported by the Shenzhen Science and Technology Program, China (Grant No. KJZD20231023100459001), Natural Science Foundation of Guangdong Province, China (Grant No. 2024A1515011731), and Shenzhen Science and Technology Program, China (Grant No. WDZC20231128135104001).

Supplementary material

Supplementary material associated with this article can be found in the online version at 10.1016/j.oceaneng.2025.124030.

Appendix A. Considered sea state

Table A.1
Time-involved sea state definition.

Case	Parameters	Stage 1		CP1	Stage 2		CP2	Stage 3		CP3	Stage 4	
		$\kappa = 1$	$\kappa = 2$	(min)	$\kappa = 1$	$\kappa = 2$	(min)	$\kappa = 1$	$\kappa = 2$	(min)	$\kappa = 1$	$\kappa = 2$
1	H_s(m)	1.81	0.76	13	1.72	0.69	27	1.37	0.7	45	1.52	0.73
	β_p(°)	237.2	109.7		215.3	87.2		175.4	71.7		153.3	58.1
	T_p(s)	7.3	12.5		8	13.2		8.7	13.8		8.8	13.5
	s	17	45		17	45		20	40		20	40
2	H_s(m)	1.52	0.67	18	1.68	0.69	32	1.7	0.7	46	1.68	0.73
	β_p(°)	124.6	78.4		141.5	88.7		153.1	98.7		172.3	118.1
	T_p(s)	6.9	12.5		8.3	13.2		8.7	13.8		8.7	13.5
	s	19	45		19	45		22	40		22	40
3	H_s(m)	1.55	0.55	19	1.5	0.5	38	1.37	0.6	50	1.52	0.52
	β_p(°)	147.1	47		172.5	13.5		195.3	60		205.9	55
	T_p(s)	12.1	12.4		11.8	13		11.1	13.8		10.6	13.6
	s	19	39		19	39		20	50		20	50
4	H_s(m)	1.22	0.42	23	1.18	0.38	37	1.25	0.45	49	1.2	0.4
	β_p(°)	273.2	194.7		293.5	186.2		255.5	174.4		237.7	138.9
	T_p(s)	6.5	11.5		7	11.8		7.5	10.9		6.8	10.8
	s	23	40		23	40		21	49		21	49
5	H_s(m)	1.64	0.58	16	1.57	0.51	25	1.7	0.65	37	1.62	0.55
	β_p(°)(s)	78	221.5		108.1	200.5		113.1	251.5		162.3	238.7
	T_p(s)	8.3	10.8		10.5	10.5		11.3	11.7		11.7	11.6
	s	20	56		20	56		17	48		17	48
6	H_s(m)	1.27	0.48	22	1.2	0.41	39	1.3	0.53	50	1.24	0.44
	β_p(°)(s)	97.4	38.6		134	82		170	92		192.5	68
	T_p(s)	9.9	10.2		10.5	11.6		10.6	12.5		11.3	12.6
	s	20	39		20	39		22	46		22	46
7	H_s(m)	1.67	0.52	25	1.59	0.44	37	1.75	0.65	40	1.69	0.57
	β_p(°)	75.4	120.2		120.5	132.1		155.2	159.4		185.5	134.7
	T_p(s)	11.1	11.5		12.6	11.7		12.4	11.9		12.5	12.1
	s	20	40		20	40		18	55		18	55
8	H_s(m)	1.28	0.45	29	1.2	0.37	42	1.37	0.54	51	1.32	0.49
	β_p(°)	38.9	289.2		59.5	215.6		72.3	151.5		55.7	210.5
	T_p(s)	6.4	13.8		7.2	14.5		8.8	14.9		8.2	13.9
	s	22	42		22	42		19	51		19	51
9	H_s(m)	1.53	0.57	7	1.45	0.49	21	1.61	0.65	42	1.55	0.59
	β_p(°)	121.9	67.3		145	77		175	92		208.9	88.9
	T_p(s)	5.6	11.7		6.7	11.7		6.9	12.5		7.8	12.5
	s	17	48		17	48		21	42		21	42
10	H_s(m)	1.68	0.59	25	1.6	0.51	39	1.75	0.66	50	1.63	0.56
	β_p(°)	265.5	70.7		285	55		302.1	45.5		345	35.5
	T_p(s)	9.2	13.1		9.5	13.6		8.4	12.9		8.1	12.5
	s	19	39		19	39		17	45		17	45

Appendix B. Transfer function

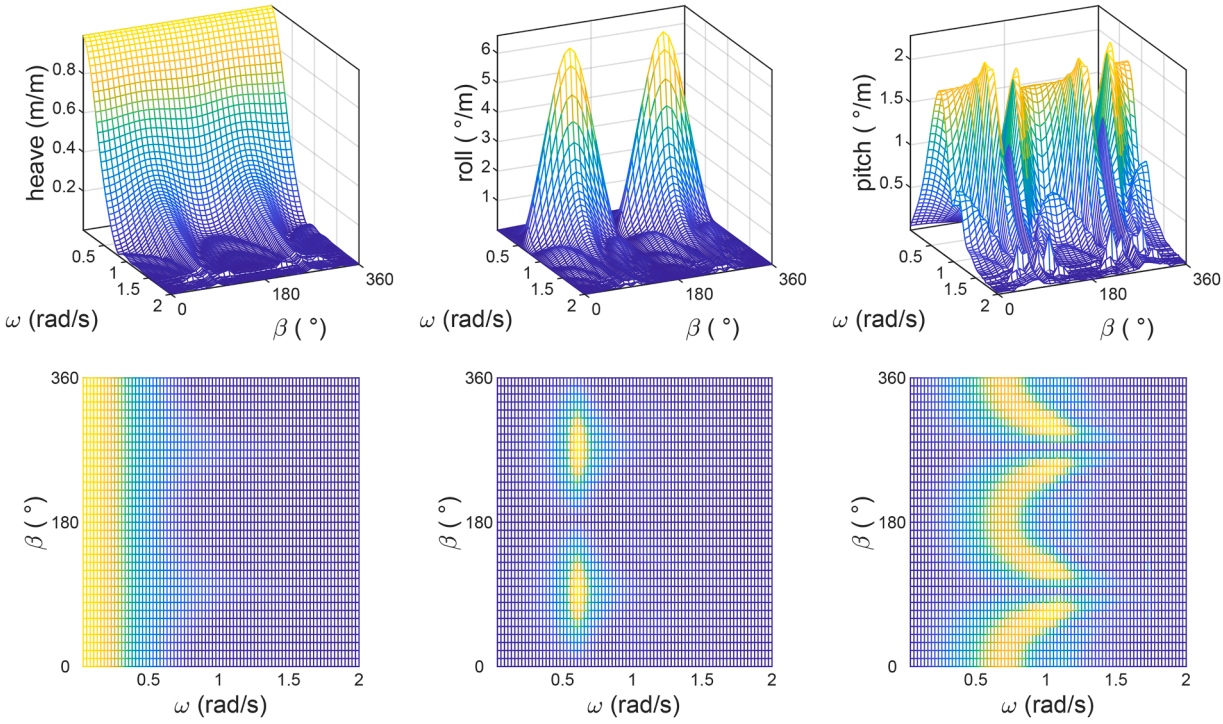

Fig. B.1. RAOs of the cargo ship.

References

Brodtkorb, A.H., Nielsen, U.D., 2023. Automatic sea state estimation with online trust measure based on ship response measurements. Contr. Eng. Pract. 130, 105375. https://doi.org/10.1016/j.conengprac.2022.105375

Chen, X., Okada, T., Kawamura, Y., Mitsuyuki, T., et al., 2020. Estimation of on-site directional wave spectra using measured hull stresses on 14,000 TEU large container ships 25 (3), 690–706. https://doi.org/10.1007/s00773-019-00673-w

Chen, X., Okada, T., Kawamura, Y., Mitsuyuki, T., 2021. Estimation of directional wave spectra and hull structural responses based on measured hull data on 14,000 TEU large container ships 80, 103087. https://doi.org/10.1016/j.marstruc.2021.103087

Cheng, X., Li, G., Skulstad, R., Chen, S., Hildre, H.P., Zhang, H., 2019. Modeling and analysis of motion data from dynamically positioned vessels for sea state estimation. In: 2019 International Conference on Robotics and Automation (ICRA). IEEE, pp. 6644–6650. https://doi.org/10.1109/ICRA.2019.8794069

Fossen, T.I., 2011. Handbook of Marine Craft Hydrodynamics and Motion Control. John Wiley & Sons.

Han, P., Li, G., Cheng, X., Skjong, S., Zhang, H., 2022a. An uncertainty-aware hybrid approach for sea state estimation using ship motion responses. IEEE Trans. Indus. Inf. 18 (2), 891–900. https://doi.org/10.1109/TII.2021.3073462

Han, P., Li, G., Skjong, S., Zhang, H., 2022b. Directional wave spectrum estimation with ship motion responses using adversarial networks. Mar. Struct. 83, 103159. https://doi.org/10.1016/j.marstruc.2022.103159

Han, X., Leira, B.J., Sævik, S., Ren, Z., 2021. Onboard tuning of vessel seakeeping model parameters and sea state characteristics. Mar. Struct. 78, 102998. https://doi.org/10.1016/j.marstruc.2021.102998

Huang, W., Liu, X., Gill, E., 2017. Ocean wind and wave measurements using X-band marine radar: a comprehensive review. Remote Sens. 9 (12), 1261. https://doi.org/10.3390/rs9121261

Iseki, T., Ohtsu, K., 2000. Bayesian estimation of directional wave spectra based on ship motions. Contr. Eng. Pract. 8 (2), 215–219. https://doi.org/10.1016/S0967-0661(99)00156-2

Kawai, T., Kawamura, Y., Okada, T., Mitsuyuki, T., Chen, X., 2021. Sea state estimation using monitoring data by convolutional neural network (CNN). J. Mar. Sci. Technol. 26 (3), 947–962. https://doi.org/10.1007/s00773-020-00785-8

Killick, R., Fearnhead, P., Eckley, I.A., 2012. Optimal detection of changepoints with a linear computational cost. J. Am. Stat. Assoc. 107 (500), 1590–1598. 1101.1438. https://doi.org/10.1080/01621459.2012.737745

Kim, H., Kang, H., Kim, M.-H., 2019. Real-time inverse estimation of ocean wave spectra from vessel-motion sensors using adaptive Kalman filter. Appl. Sci. 9 (14), 2797. https://doi.org/10.3390/app9142797

Ma, C., Hu, Z.-Z., Zheng, X.Y., Ren, Z., 2024. Inertia load reduction for loadoff during floating offshore wind turbine installation: Release decision and ballast control. Sustainable Horiz. 10, 100096. https://doi.org/10.1016/j.horiz.2024.100096

Majidian, H., Wang, L., Enshaei, H., 2022. Part. A: a review of the real-time sea-state estimation, using wave buoy analogy. Ocean Eng. 266, 111684. https://doi.org/10.1016/j.oceaneng.2022.111684

Martin, S., 2014. An Introduction to Ocean Remote Sensing. Cambridge University Press, Cambridge. 2 edition. https://doi.org/10.1017/CBO9781139094368

Mas-Soler, J., Simos, A.N., 2020. A Bayesian wave inference method accounting for nonlinearity related inaccuracies in motion RAOs. Appl. Ocean Res. 99, 102125. https://doi.org/10.1016/j.apor.2020.102125

Mittendorf, M., Nielsen, U.D., Bingham, H.B., Storhaug, G., 2022. Sea state identification using machine learning—a comparative study based on in-service data from a container vessel. Mar. Struct. 85, 103274. https://doi.org/10.1016/j.marstruc.2022.103274

Mounet, R. E.G., Nielsen, U.D., Brodtkorb, A.H., 2023. Doppler shift approximation for predicting the wave-induced response of advancing vessels in following waves. In: ASME 2023 42nd International Conference on Ocean, Offshore and Arctic Engineering. American Society of Mechanical Engineers Digital Collection. https://doi.org/10.1115/OMAE2023-107733

Newman, J.N., 2018. Marine Hydrodynamics. The MIT Press.

Nielsen, U.D., 2008. Introducing two hyperparameters in Bayesian estimation of wave spectra. Probab. Eng. Mech. 23 (1), 84–94. https://doi.org/10.1016/j.probengmech.2007.10.007

Nielsen, U.D., 2017. Transformation of a wave energy spectrum from encounter to absolute domain when observing from an advancing ship. Appl. Ocean Res. 69, 160–172. https://doi.org/10.1016/j.apor.2017.10.011

Nielsen, U.D., Bingham, H.B., Brodtkorb, A.H., Iseki, T., Jensen, J.J., Mittendorf, M., Mounet, R. E.G., Shao, Y., Storhaug, G., Sørensen, A.J., Takami, T., 2023a. Estimating waves via measured ship responses. Sci. Rep. 13 (1), 17342. https://doi.org/10.1038/s41598-023-44552-2

Nielsen, U.D., Brodtkorb, A.H., Sørensen, A.J., 2019. Sea state estimation using multiple ships simultaneously as sailing wave buoys. Appl. Ocean Res. 83, 65–76. https://doi.org/10.1016/j.apor.2018.12.004

Nielsen, U.D., Dietz, J., 2020. Estimation of sea state parameters by the wave buoy analogy with comparisons to third generation spectral wave models. Ocean Eng. 216, 107781. https://doi.org/10.1016/j.oceaneng.2020.107781

Nielsen, U.D., Iwase, K., Mounet, R. E.G., 2024. Comparing machine learning-based sea state estimates by the wave buoy analogy. Appl. Ocean Res. 149, 104042. https://doi.org/10.1016/j.apor.2024.104042

Nielsen, U.D., Mittendorf, M., Shao, Y., Storhaug, G., 2023b. Wave spectrum estimation conditioned on machine learning-based output using the wave buoy analogy. Mar. Struct. 91, 103470. https://doi.org/10.1016/j.marstruc.2023.103470

Pascoal, R., Guedes Soares, C., 2009. Kalman filtering of vessel motions for ocean wave directional spectrum estimation. Ocean Eng. 36 (6), 477–488. https://doi.org/10.1016/j.oceaneng.2009.01.013

Pascoal, R., Perera, L.P., Guedes Soares, C., 2017. Estimation of directional sea spectra from ship motions in sea trials. Ocean Eng. 132, 126–137. https://doi.org/10.1016/j.oceaneng.2017.01.020

Peng, X., Zhang, B., Rong, L., 2019. A robust unscented Kalman filter and its application in estimating dynamic positioning ship motion states. J. Mar. Sci. Technol. 24 (4), 1265–1279. https://doi.org/10.1007/s00773-019-00624-5

Ren, Z., Han, X., Verma, A.S., Dirdal, J.A., Skjetne, R., 2021a. Sea state estimation based on vessel motion responses: Improved smoothness and robustness using Bézier surface and L1 optimization. Mar. Struct. 76, 102904. https://doi.org/10.1016/j.marstruc.2020.102904

Ren, Z., Skjetne, R., Verma, A.S., Jiang, Z., Gao, Z., Halse, K.H., 2021b. Active heave compensation of floating wind turbine installation using a Catamaran construction vessel. Mar. Struct. 75, 102868. https://doi.org/10.1016/j.marstruc.2020.102868

Ren, Z., Verma, A.S., Li, Y., Teuwen, J. J.E., Jiang, Z., 2021c. Offshore wind turbine operations and maintenance: A state-of-the-art review. Renewable Sustainable Energy Rev. 144, 110886. https://doi.org/10.1016/j.rser.2021.110886

Sifuzzaman, M., 2009. Application of wavelet transform and its advantages compared to fourier transform. In: Journal of Physical Science. 13, 121–134.

SINTEF, SIMA: simulation of marine operations. https://sima.sintef.no/. Accessed: 2024-09-23.

Skjetne, R., Ren, Z., 2020. A survey on modeling and control of thruster-assisted position mooring systems. Mar. Struct. 74, 102830.

Takami, T., Dam Nielsen, U., Juncher Jensen, J., Maki, A., Matsui, S., Komoriyama, Y., 2024. Onboard identification of stability parameters including nonlinear roll damping via phase-resolved wave estimation using measured ship responses. Mech. Syst. Signal Process. 210, 111166. https://doi.org/10.1016/j.ymssp.2024.111166

Takami, T., Nielsen, U.D., Jensen, J.J., Chen, X., et al., 2023. Estimation of encountered wave elevation sequences based on response measurements in multi-directional seas 135, 103570. https://doi.org/10.1016/j.apor.2023.103570

Takami, T., Nielsen, U.D., Xi, C., Jensen, J.J., Oka, M., et al., 2022. Reconstruction of incident wave profiles based on short-time ship response measurements 123, 103183. https://doi.org/10.1016/j.apor.2022.103183

Tannuri, E.A., Sparano, J.V., Simos, A.N., Da Cruz, J.J., 2003. Estimating directional wave spectrum based on stationary ship motion measurements. Appl. Ocean Res. 25 (5), 243–261. https://doi.org/10.1016/j.apor.2004.01.003

Tu, F., Ge, S.S., Choo, Y.S., Hang, C.C., 2018. Sea state identification based on vessel motion response learning via multi-layer classifiers. Ocean Eng. 147, 318–332. https://doi.org/10.1016/j.oceaneng.2017.08.047

Wang, J., Shi, W., Ren, Y., Ran, X., Collu, M., Venugopal, V., Zhao, H., 2025. An integrated multi-objective optimization framework for large-scale floating offshore wind turbine. Renewable Energy 258, 124978.

Yan, C., Shi, W., Jiang, Z., Li, L., Han, X., Li, X., 2025. Reliability-based design optimization of a mooring system for a floating wind turbine. Renewable Energy 260, 125116.

Zhang, T., Chen, S., Ma, C., Ren, Z., 2024. Ship as a buoy: RAO-driven heading adjustment strategy based on restricted isometry property. In: ASME 2024 43rd International Conference on Ocean, Offshore and Arctic Engineering. American Society of Mechanical Engineers Digital Collection. https://doi.org/10.1115/OMAE2024-122159

Zhang, T., Ren, Z., 2025. Restricted isometry property in wave buoy analogy and application to multispectral fusion, https://doi.org/10.1109/TITS.2024.3519199